International Journal of Applied Power Engineering (IJAPE)
Vol. 1, No. 2, August 2012, pp. 47~64
ISSN: 2252-8792

Dynamic Modeling of Autonomous Wind–Diesel system with Fixed-Speed Wind Turbine

Najafi Hamid Reza[1], Dastyar. Farshad [2]
[1]Faculty of Electrical and Computer Engineering, University of Birjand, IRAN
[2]MonenCo Iran consulting engineers (MAPNA GROUP), IRAN

Article Info

Article history:

Received Mar 22, 2012
Revised Jul 10, 2012
Accepted Jul 16, 2012

Keyword:

Dynamic Modeling
Fixed-Speed Wind Turbine
Saddle node bifurcation
Hopf bifurcation
participation factor

ABSTRACT

Wind turbines have often connected to small power systems, operating in parallel to diesel generators, as is typically the case in autonomous wind–diesel installations or small island systems with high wind potential. Hence, the modeling and analysis of the dynamic behavior of wind–diesel power systems in presence of wind power will be important. In this paper, the system under study is modeled by a set of dynamic and algebraic equations (DAE). Dynamic behavior of a wind-diesel system is investigated by the proposed dynamic model. Wind-diesel system consists of wind turbines that are connected to synchronous diesel generator via short transmission line with local load. Dynamic stability of autonomous wind–diesel systems are discussed with emphasis on the eigenvalue analysis and the effective parameters on system stability. In this regards, saddle node bifurcation and hopf bifurcation are also investigated.

Copyright © 2012 Institute of Advanced Engineering and Science.
All rights reserved.

Corresponding Author:

Najafi .Hamid Reza
Faculty of Electrical and Computer Engineering, University of Birjand, IRAN
Email: h.r.najafi@birjand.ac.ir

1. INTRODUCTION

As result of environmental concern, the penetration of renewable power in power systems is increasing. Wind energy is one way of electrical generation from renewable sources that uses wind turbines to convert the energy contained in flowing air into electrical energy. Wind power is the world's fastest growing energy source with a average growth over the past 7 years of 26% and a foreseeable penetration 12% of global electricity demand by 2020 [1]. In many countries wind power expands, and covers a steadily increasing part of these countries power demand. This development is due to strong worldwide available wind resources, environmental concerns, and the improved cost efficiency of new wind technologies. As more and more attention is paid to the increase of wind farm, a number of problems should be investigated in more detail especially in weak systems.

Increasing of wind farms penetration in power system justifies the need for development of accurate wind turbine model, evaluating their influence and thus improving the planning and exploitation of electrical network. Actually, one of the used wind farm concepts in power systems is based on fixed speed wind turbines with directly grid coupled squirrel cage induction generator connected to the wind turbine rotor through gearbox. This generator presents very small rotational speed variations because of the only speed variations that can occur are changes in the rotor slip, and therefore these wind turbines are considered to operate at fixed speed. A squirrel cage induction generator consumes reactive power, and therefore compensating capacitors are added to generate the induction generator magnetizing current, thus improving the power factor. The dynamic behavior of wind farms has been usually represented by a suitable model, including the modeling of all wind turbines and the internal electrical network [2–4]. But Wind turbines are often connected to small power systems. The objective is always to maximize the wind penetration, while maintaining an acceptable level of service quality to the consumers and ensuring good dynamic response characteristics and a sufficient stability margin in case of disturbances. A variety of operating and control problems associated with the wind–diesel systems have been identified and studied in the relevant literature. Each type of problem requires a different modeling approach and poses widely varying analysis requirements [5]. The modeling and analysis of the dynamic behavior of wind–diesel power systems has been the subject of numerous publications (e.g. [6–15]), dealing both with small autonomous installations and relatively larger systems, comprising a conventional power station and multiple wind turbines or wind farms.

Dynamic modeling of wind-diesel system have not carefully discussed in recent literatures. In this paper a complete dynamic model is presented for an autonomous wind–diesel system and the dynamic stability of a sample system is discussed in detail with emphasis on the modal analysis.

The rest of this paper is organized as follows: section 2 describes system components modeling. Section 3 explains rotor reference frame quantities transformation to the stator-flux oriented reference frame. Differential-algebraic equations (DAE) of system are presented in section 4 and after verification of proposed model by simulation, dynamic stability of study system are studied in details. Conclusions are finally made in section 5.

2. SYSTEM COMPONENTS AND MODELING

The single line diagram of the sample system is depicted in Figure 1.The complete model of study system is constructed from a number of components. The sample system consists of a wind farm with fixed speed wind turbines implemented with squirrel cage induction generators that are connected to a 1.5 MW diesel generator through a short transmission line. Compensating capacitor bank and local load are connected to the wind farm bus and local load bus respectively. Multiple wind turbines in the wind farm are required to aggregate. For the dynamic stability study, an aggregated model is sufficient to represent the entire wind farm at point of common coupling. The system parameters are given in appendix A. The models of system components are illustrated in the following sub-sections.

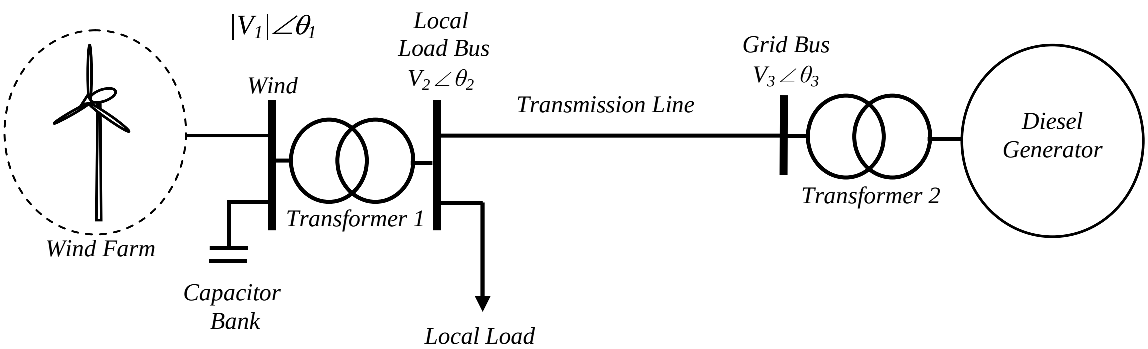

Figure 1. Single line diagram of the sample system

2.1 Wind turbine model

The behavior of wind turbine can be represented by modeling the rotor and drive train. Applying the actuator disk theory [16, 17], the rotor model provides the aerodynamic torque extracted from the wind by the following equation:

$$T_w = \frac{1}{2}\rho\pi R^3 V_w{}^2 \frac{C_P(\lambda,\beta)}{\lambda} \tag{1}$$

Where ρ (kg/m3) is the air density, R (m) is the rotor disk radius or blade length; Vw (m/s) is the wind speed and Cp (λ, β) is the power coefficient which is a function of the tip speed ratio λ and the blade pitch angle β for pitch regulated wind turbines that is supposed in this paper and Cp (λ, β) is [17]:

$$C_p(\lambda,\beta) = c_1\left(\frac{c_2}{\lambda_i} - c_3\beta - c_4\right)e^{\frac{-c_5}{\lambda_i}} + c_6\lambda \tag{2}$$

Where:

$$\frac{1}{\lambda_i} = \frac{1}{\lambda + 0.08\beta} - \frac{0.035}{\beta^3 + 1} \tag{3}$$

Representative values of c_i coefficients are:

$$c_1 = 0.5176, c_2 = 116, c_3 = 0.4, c_4 = 5, c_5 = 21, c_6 = 0.0068.$$

The maximum value of C_p ($c_{pmax} = 0.48$) is achieved for $\beta=0$ degree and for $\lambda=8.1$. This particular value of λ is defined as the nominal value (λ_nom) .The tip speed ratio is defined as:

$$\lambda = \frac{R\,\omega_t}{V_w} \tag{4}$$

where ω_t (rad/s) is the blade angular speed.

2.2 Drive train model

The drive train model is usually represented by two masses [18, 19] as shown in Figure 2.

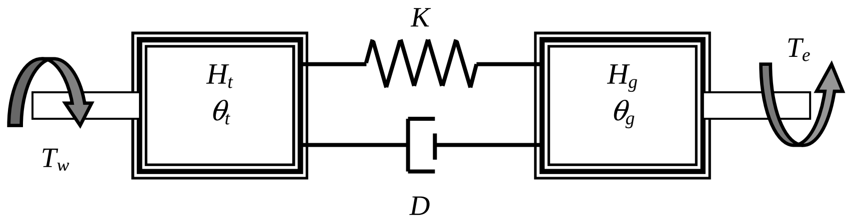

Figure 2. Drive train model

The first mass stands for the wind turbine rotor (blades, hub and low-speed shaft), while the second mass stands for generator rotor (high-speed shaft). The equations of the two-mass model in per unit are given here:

$$2H_t \frac{d}{dt}(\omega_t) = T_w - K(\theta_{tg}) - D(\omega_t - (1-S)\omega_S) \tag{5}$$

$$-2H_g\, \omega_s \frac{d}{dt}(S) = K(\theta_{tg}) + D(\omega_t - (1-S)\omega_S) - T_e \tag{6}$$

$$\frac{d}{dt}(\theta_{tg}) = \omega_t - \omega_g = \omega_t - (1-S)\omega_S \tag{7}$$

Where θ_{tg} is the angle between the turbine rotor and the generator rotor, ω_t, ω_g, H_t and H_g are the turbine and generator rotor angular speed and inertia constant, respectively. K and D are the drive train stiffness and damping constants, respectively. T_w is the torque provided by the wind and T_e is the electromagnetic torque. All parameters are in per unit.

2.3 Pitch angle control model

A Proportional-Integral (PI) controller is used to control the blade pitch angle in order to limit the electric output power to the nominal mechanical power. The pitch angle is kept constant at zero degree when the measured electric output power is under its nominal value. When it increases above its nominal value, the PI controller increases the pitch angle to bring back the measured power to its nominal value. The control system is illustrated in the Figure 3.

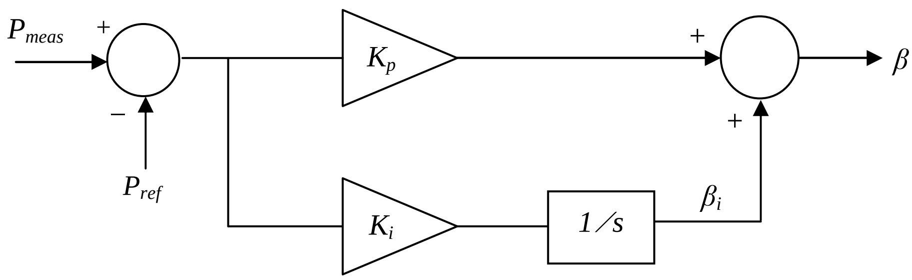

Figure 3. Control scheme of pitch regulated wind turbines

Mathematical description of pitch control block is given below:

$$\beta = K_P(P_{meas} - P_{ref}) + \beta_i \tag{8}$$

$$\beta_i = K_i \int (P_{meas} - P_{ref})\, dt \tag{9}$$

$$\frac{d}{dt}(\beta_i) = K_i (P_{meas} - P_{ref}) \tag{10}$$

Where K_P and K_i are the PI controller gains, P_{ref} and P_{meas} are the reference power and output power of wind turbine respectively.

2.4 SCIG model

Two main induction generator models are used when performing power system dynamic studies:

- A detailed model which includes electromagnetic transients both in the stator and the rotor circuits, containing four electromagnetic state variables.
- A simplified model that neglects stator transients, containing two electromagnetic state variables. The later model is sometimes referred in the literatures as the third order model, accounting for the two electric state variables and the generator speed. Hence, the detailed model is referred as the fifth order model. This paper uses a well-known simplified model by neglecting stator flux linkage transients that is common when performing stability studies [21, 22]. Thus the differential equations of induction generator model can be expressed by:

$$\frac{d}{dt}(e'_d) = -\frac{1}{T'_o}[e'_d - (X_{si} - X'_{si})i_{qs}] + S\,\omega_S\,e'_q \tag{11}$$

$$\frac{d}{dt}(e'_q) = -\frac{1}{T'_o}[e'_q + (X_{si} - X'_{si})i_{ds}] - S\,\omega_S\,e'_d \tag{12}$$

Where:

$$T'_o = \frac{X_{ri} + X_{mi}}{\omega_S\,R_{ri}} \tag{13}$$

$$X'_{si} = (X_{si} + X_{mi}) - \frac{X_{mi}^2}{X_{ri} + X_{mi}} \tag{14}$$

The generator electrical torque is calculated as:

$$T_e = e'_d i_{ds} + e'_q i_{qs} \tag{15}$$

where e'_d and e'_q are the d-q components of the internal equivalent thevenin voltage, i_{ds} and i_{qs} are the stator current components , T'_o is the open circuit transient time constant , X'_{si} is the transient reactance , X_{si} and X_{ri} are the stator and rotor leakage reactance's and X_{mi} is the magnetizing reactance. The sub indexes *s*, *r* and *i* stand for the rotor, stator and induction generator quantities, respectively, and the sub indexes *d*, *q* stand for the components aligned with the d- and q- axis. *S* is the slip of induction generator defined as $S = (\omega_s - \omega_g)/\,\omega_s$ while variables ω_s and ω_g are the synchronous and generator rotor angular speed, respectively. All variables are in per unit value.

2.5 Dynamic model of the synchronous generator

The full detailed mathematical model of a synchronous machine takes into account several effects introduce by different rotor circuits, and consist of seven nonlinear differential equations for each machine. In stability study, the complete mathematical description is complicated, unless some simplifications were used [21, 23, 24, and 25]. Neglecting the stator transient and damper winding are common simplification assumptions. In this paper suppositions are used, in other words, the two axis model is employed in the modeling and the saturation effect is neglected [25]. The voltage equations of a synchronous generator in the d-q reference frame (as shown in Figure 4) are given by:

$$\frac{d}{dt}(E'_q) = \frac{1}{T'_{do}}[-E'_q - (x_d - x'_d)I_d + E_{fd}] \tag{16}$$

$$\frac{d}{dt}(E'_d) = \frac{1}{T'_{qo}}[-E'_d + (x_q - x'_q)I_q] \tag{17}$$

$$V_3 e^{j\theta_3} + (R_S + jx'_d)(I_d + jI_q)e^{j[\delta - \frac{\pi}{2}]} - [E'_d + (x'_q + x'_d)I_q + jE'_q)]e^{j(\delta - \frac{\pi}{2})} = 0 \tag{18}$$

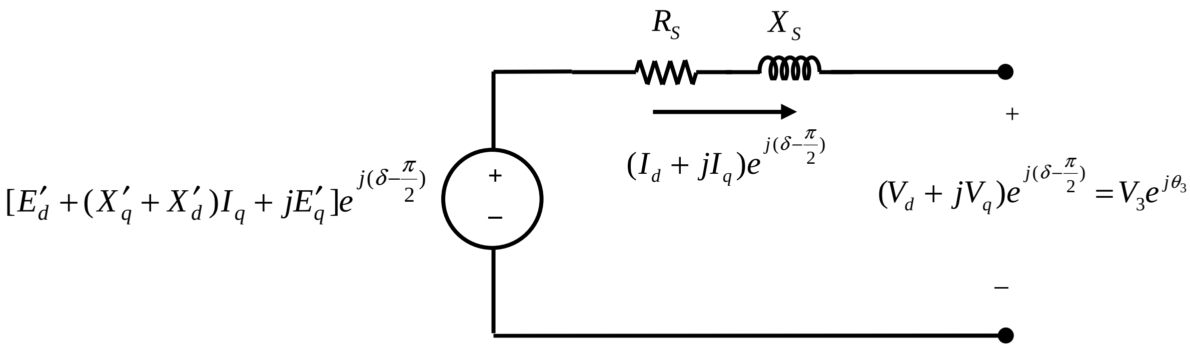

Figure 4. Dynamic equivalent circuit of synchronous generator (two-axis model)

Differential equation of the excitation system is derived directly from Figure 5. This figure shows a simple static exciter.

$$T_{ex} \frac{d}{dt}(E_{fd}) = K_{ex}(V_{ref} - V_3) - E_{fd} \tag{19}$$

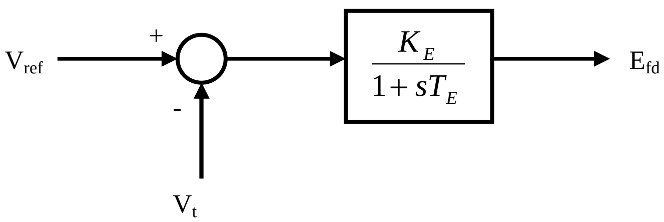

Figure 5. Block diagram of a static exciter

Mechanical equations are given by:

$$\frac{2H}{\omega_S} \frac{d}{dt}(\omega) = T_M - E'_d I_d - E'_q I_q - (x'_q - x'_d) I_d I_q - D(\omega - \omega_S) \tag{20}$$

$$\frac{d}{dt}(\delta) = \omega - \omega_S \tag{21}$$

Where, E'_d and E'_q are the internal voltage components of the equivalent Thevenin. I_d and I_q, the stator current components, T'_{do} is the d-axis transient open circuit time constant , T'_{qo} is the q-axis transient open circuit time constant , E_{fd} is the excitation voltage, x_d , x_q are the reactance components , x'_d and x'_q are the transient reactance components , R_S is the stator resistance, V_3 and V_{ref} are the terminal voltage and reference voltage respectively, K_{ex}, T_{ex} are the excitation system parameters, D and H are the damping constant and inertia constant respectively, T_M and ω are the input mechanical torque and synchronous machine speed respectively. In this paper, local load is modeled by a constant impedance load.

3. TRANSFORMATION OF SYSTEM VARIABLES TO A COMMON REFERENCE FRAME

Since, study system has two machines, all system variables must be referred to a common reference frame. In this paper, stator reference frame is chosen as a common reference frame.

3.1 SCIG rotor reference frame quantities

Transformation matrix from SCIG rotor reference frame (d-q) to the stator-flux oriented reference frame (D-Q) and transition angle are given by:

$$\begin{bmatrix} F_{d,IM} \\ F_{q,IM} \end{bmatrix} = \begin{bmatrix} \sin(\theta) & -\cos(\theta) \\ \cos(\theta) & \sin(\theta) \end{bmatrix} \begin{bmatrix} F_{D,IM} \\ F_{Q,IM} \end{bmatrix} \tag{22}$$

$$\theta = \int (\omega_g - \omega_S) dt \tag{23}$$

At above equations, $F_{d,IM}$ and $F_{q,IM}$ are the quantities of induction machine (SCIG) rotor reference frame, $F_{D,IM}$ and $F_{Q,IM}$ are transformed quantities at the stator-flux oriented reference frame. The diagram of such transformation is shown in Figure 6.

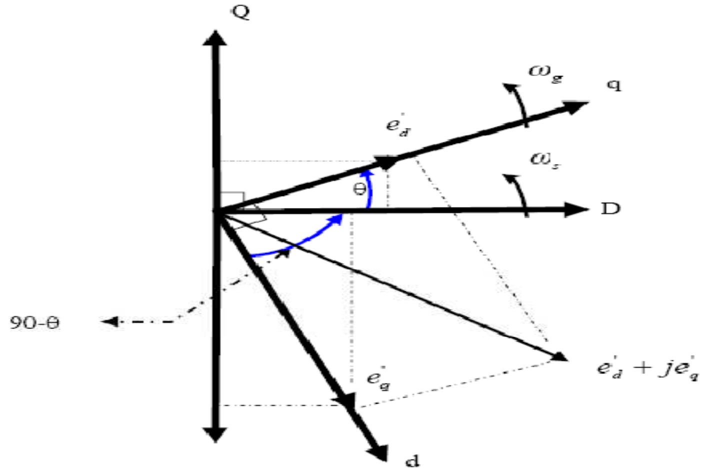

Figure 6. Schematic diagram of SCIG quantities transformation

After this transformation, the SCIG dynamic equations can be obtained as follow:

$$\frac{d}{dt}(e'_D) = -\frac{1}{T'_o}[e'_D - (X_{si} - X'_{si}) I_{QS}] + 2S\,\omega_S\, e'_Q \tag{24}$$

$$\frac{d}{dt}(e'_Q) = -\frac{1}{T'_o}[e'_Q + (X_{si} - X'_{si}) I_{DS}] - 2S\,\omega_S\, e'_D \tag{25}$$

$$T_e = e'_D I_{DS} + e'_Q I_{QS} \tag{26}$$

Equivalent circuit of SCIG in stator-flux oriented reference frame is depicted in Figure 7.

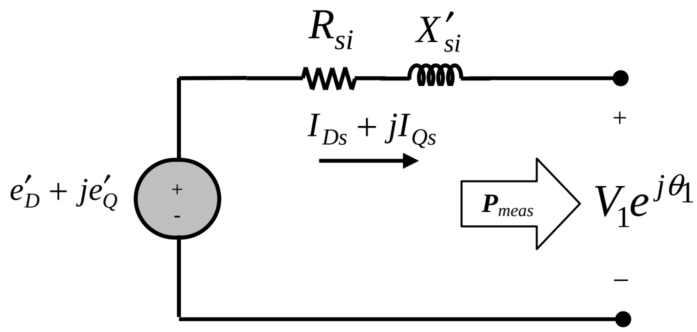

Figure 7. Equivalent circuit of SCIG in stator-flux oriented reference frame

Algebraic equations of equivalent circuit of SCIG are given by:

$$e'_D = R_{si} I_{DS} - X'_{si} I_{QS} + V_1 \cos(\theta_1) \tag{27}$$

$$e'_Q = R_{si} I_{QS} + X'_{si} I_{DS} + V_1 \sin(\theta_1) \tag{28}$$

Where, R_{si} is the stator resistance of induction generator. Output power of wind turbine is given by:

$$P_{meas} = \mathrm{Re}\{V_1 e^{j\theta_1}.(I_{DS} + jI_{QS})^*\} = V_1\cos(\theta_1)I_{DS} + V_1\sin(\theta_1)I_{QS} \tag{29}$$

3.2 Synchronous machine rotor reference frame quantities

Transformation matrix from rotor reference frame (d-q) to the stator-flux oriented reference frame (D-Q) for synchronous machine (SM) and transition angle are given by:

$$\begin{bmatrix} F_{d,SM} \\ F_{q,SM} \end{bmatrix} = \begin{bmatrix} \sin(\delta) & -\cos(\delta) \\ \cos(\delta) & \sin(\delta) \end{bmatrix} \begin{bmatrix} F_{D,SM} \\ F_{Q,SM} \end{bmatrix} \tag{30}$$

$$\delta = \int(\omega - \omega_S)dt \tag{31}$$

Where $F_{d,SM}$ and $F_{q,SM}$ are the quantities of rotor reference frame, $F_{D,SM}$ and $F_{Q,SM}$ are quantities of the stator-flux oriented reference frame. The diagram of such transformation is shown in Figure 8.

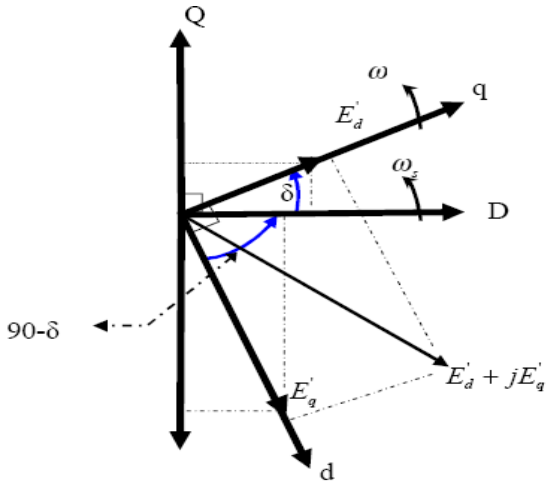

Figure 8. Schematic diagram of quantities transformation

Thus, the synchronous machine dynamic equations at common reference frame are:

$$\begin{aligned} \frac{d}{dt}(E_D') = & -E_D'[\frac{\cos^2(\delta)}{T_{do}'} + \frac{\sin^2(\delta)}{T_{qo}'}] + E_Q'[\frac{\sin(2\delta)}{2}(\frac{1}{T_{qo}'} - \frac{1}{T_{do}'}) - \dot{\delta}] + I_D[\frac{x_q - x_q'}{2T_{qo}'} - \frac{x_d - x_d'}{2T_{do}'}]\sin(2\delta) \\ & + I_Q[\frac{x_d - x_d'}{T_{do}'}\cos^2(\delta) + \frac{x_q - x_q'}{T_{qo}'}\sin^2(\delta)] + \frac{E_{fd}\cos(\delta)}{T_{do}'} \end{aligned} \tag{32}$$

$$\begin{aligned} \frac{d}{dt}(E_Q') = & E_D'[\sin(2\delta)(\frac{1}{2T_{qo}'} - \frac{1}{2T_{do}'}) + \dot{\delta}] - E_Q'[\frac{\sin^2(\delta)}{T_{do}'} + \frac{\cos^2(\delta)}{T_{qo}'}] - I_D[\frac{x_d - x_d'}{T_{do}'}\sin^2(\delta) \\ & + \frac{x_q - x_d'}{T_{qo}'}\cos^2(\delta)] + I_Q[\frac{x_d - x_d'}{2T_{do}'} - \frac{x_q - x_q'}{2T_{qo}'}]\sin(2\delta) + \frac{E_{fd}\sin(\delta)}{T_{do}'} \end{aligned} \tag{33}$$

$$\frac{2H}{\omega_S}\frac{d}{dt}(\omega) = T_M - E_D'I_D - E_Q'I_Q - (x_q' - x_d')[\frac{\sin(2\delta)}{2}(I_D^2 + I_Q^2) - I_D I_Q\cos(2\delta)] - D(\omega - \omega_S) \tag{34}$$

$$\frac{d}{dt}(\delta) = \omega - \omega_S \tag{35}$$

Algebraic equations of above equations are given by:

$$E_D' = R_S I_D - x_d' I_Q + V_3\cos(\theta_3) \tag{36}$$

$$E_Q' = R_S I_Q + x_d' I_D + V_3\sin(\theta_3) \tag{37}$$

4. DYNAMIC STABILITY OF STUDY SYSTEM

Power system dynamics are commonly expressed by a differential-algebraic equation (DAE) form [24], [26] :

$$\dot{x} = f(x, y, p) \tag{38}$$

$$0 = g(x, y, p) \tag{39}$$

Where, the parameter p defines specific system configurations and operation conditions, such as loads, generation, voltage setting points, etc. The dynamic state *x* (slow modes) describes the generation dynamics of power systems. The instantaneous variables *y* (fast modes) satisfies algebraic constraint, such as power flow equations, which is implicitly assumed to have an instantaneously converging transient. We can analyze power system dynamics through eigenvalue solutions [27]. However, it is difficult to analyze and simulate the nonlinear DAE due to the instantaneous dynamic nature of algebraic constraints, which is only true in the approximation sense. Traditionally, we use implicit function theorem to solve for fast variables *y* to get a reduced model in terms of slow dynamics locally around *x*. Or we compute *y* numerically at each *x*. The reduced Jacobian matrix of DAE is often used in the analysis of power system dynamics [27], [28]. The linearized dynamic expression of DAE is as below [24], [29]:

$$\begin{bmatrix} \Delta\dot{x} \\ 0 \end{bmatrix} = J \begin{bmatrix} \Delta x \\ \Delta y \end{bmatrix} \tag{40}$$

$$J = \begin{bmatrix} f_x & f_y \\ g_x & g_y \end{bmatrix} \tag{41}$$

DAE can be reduced to an ODE (ordinary-differential equation) when g_y is nonsingular, i.e., the algebraic variable Δy can be eliminated from (40) [24].

$$\Delta\dot{x} = [f_x - f_y g_y^{-1} g_x]\Delta_x \tag{42}$$

$$A = F_x = [f_x - f_y g_y^{-1} g_x] \tag{43}$$

Where A is called the reduced Jacobian matrix (RJM) as opposed to the unreduced Jacobian matrix (UJM) *J*. The stability of an equilibrium point of the DAE system for a given *p* depends on the eigenvalues of the reduced Jacobian matrix A [24]. Through tracing the eigenvalue of matrix A, we can study the local dynamic stability of the system [24], [21]. There are two steps involved to identify the dynamic stability of power system as the parameter *p* slowly changes. First, solve and trace the equilibrium point along the path, then form RJM and analyze the eigenvalues at each equilibrium point [24], [30], [31].In this research x and y are defined as:

$$x = [x_1, x_2, ..., x_{11}]^{\tau} = [\omega_t, S, \theta_{tg}, \beta_i, e'_D, e'_Q, E'_D, E'_Q, \omega, \delta, E_{fd}]^{\tau}$$

$$y = [y_1, y_2, ..., y_{11}]^{\tau} = [\lambda, V_1, \theta_1, I_{DS}, I_{QS}, \beta, I_D, I_Q, V_2, \theta_2, V_3]^{\tau}$$

4.1 Verification of model with study system simulation

Model verification has been performed using a RJM eigenvalue and study system simulation with Matlam-Simulink software. Simulation results are shown in Figure 10 to Figure16 that include the squirrel cage induction generator slip, synchronous generator speed, voltage at 1, 2, 3 buses, active power of wind turbine, synchronous generator and load diagrams.

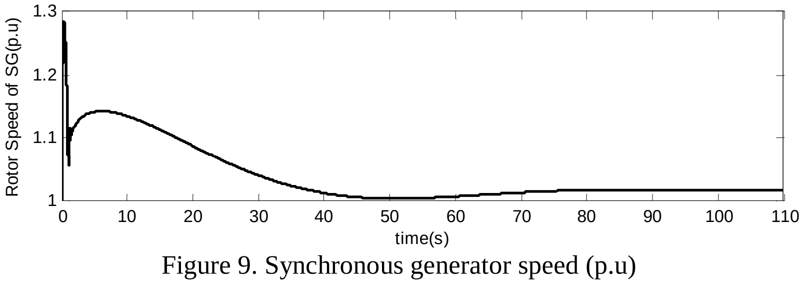

Figure 9. Synchronous generator speed (p.u)

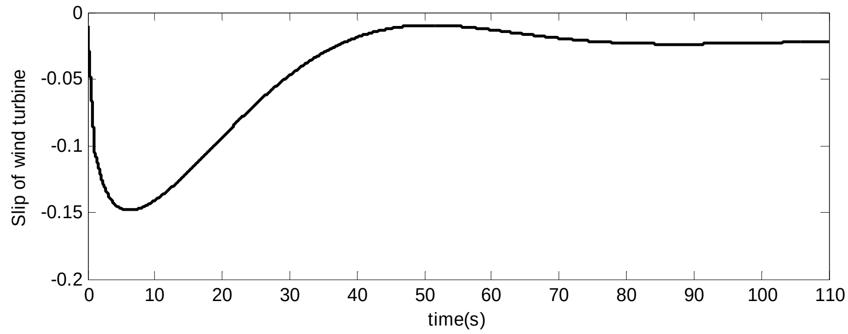

Figure 10. Squirrel cage induction generator slips (p.u)

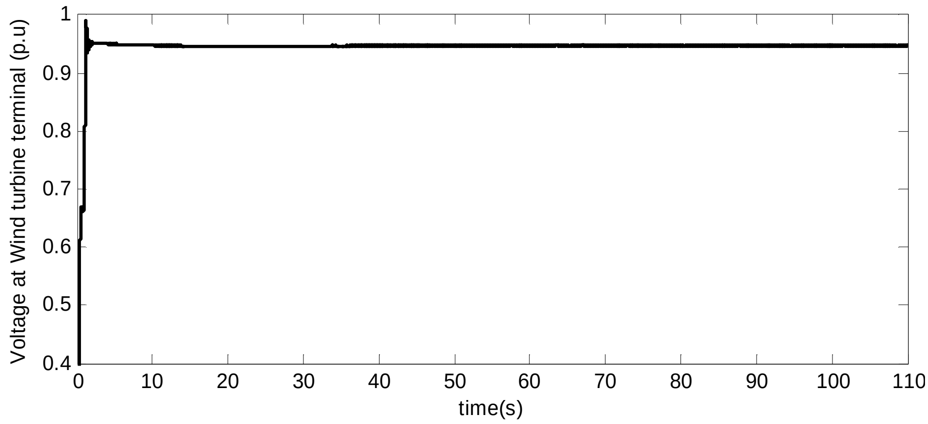

Figure 11. Voltage at wind turbine bus (p.u)

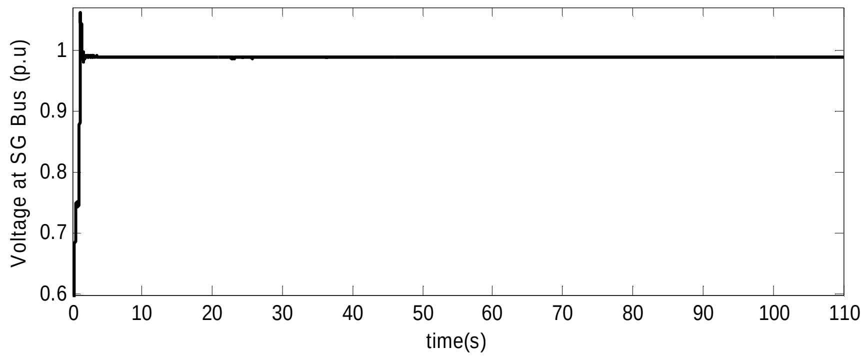

Figure 12. Voltage at synchronous generator bus (p.u)

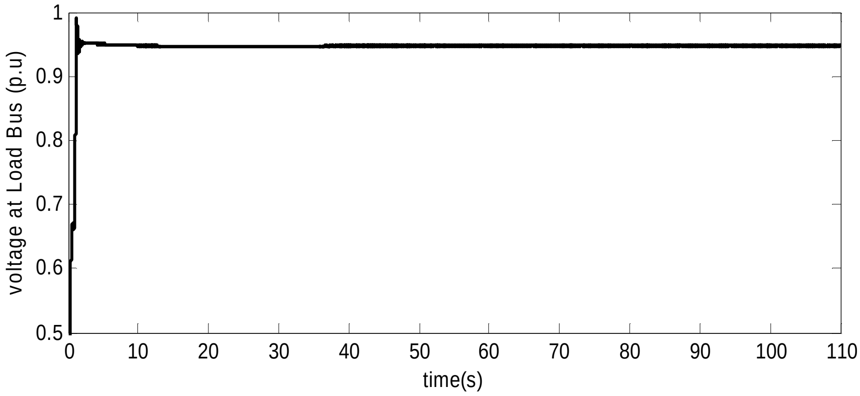

Figure 13. Voltage at load bus (p.u)

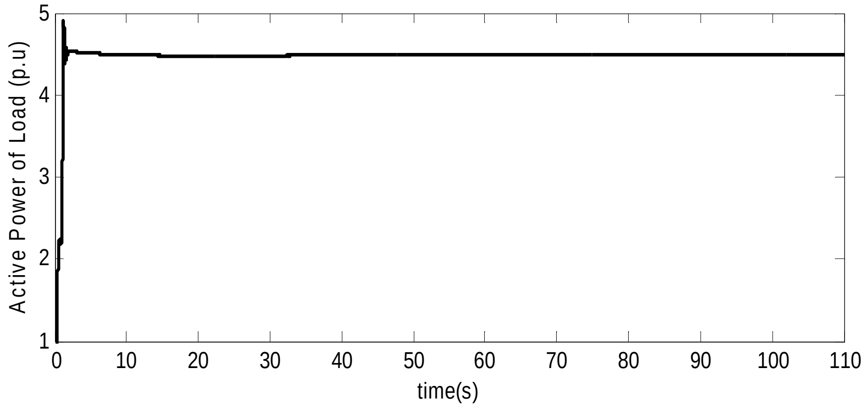

Figure 14. Active power of load (p.u)

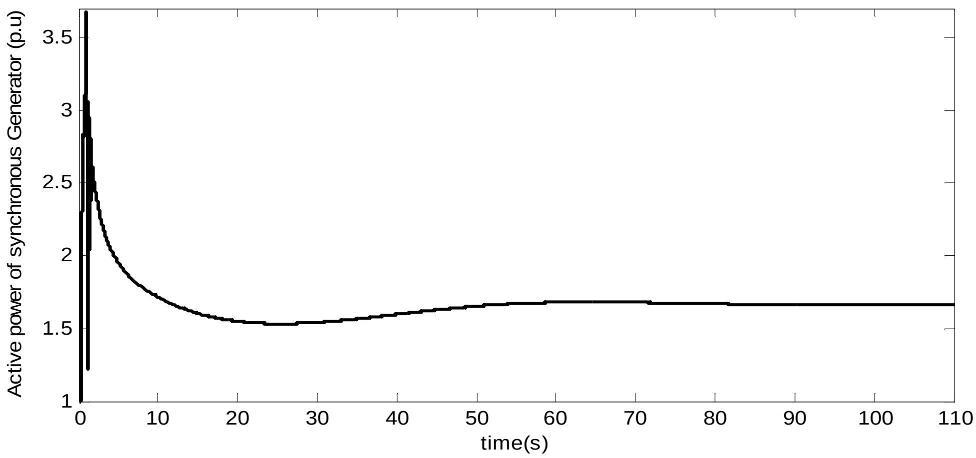

Figure 15. Active power of synchronous generator (p.u)

All figures show stable operation of study system with parameters that are presented in appendix A. In Figure 16 RJM eigenvalues are shown that all eigenvalues are in left of imaginary axis, therefore study system is stable.

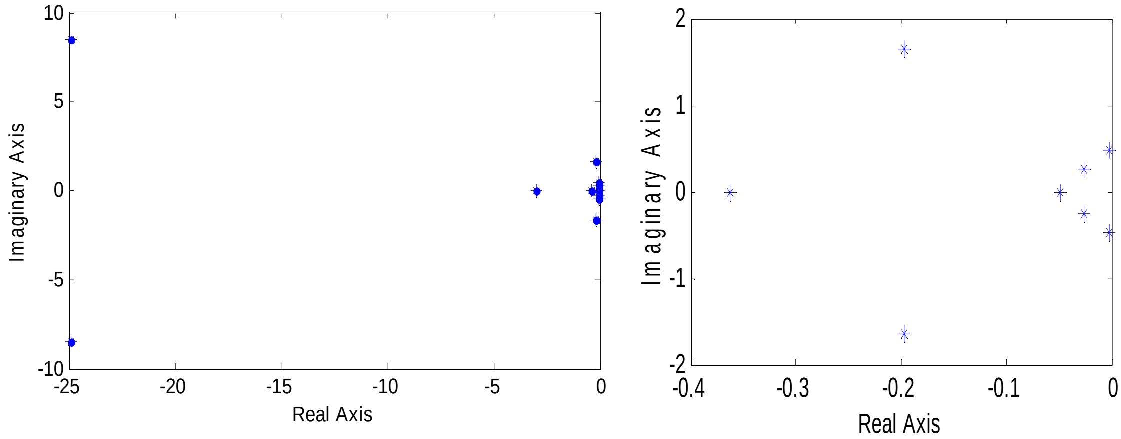

Figure 16 Eigenvalues of study system

The Jacobian matrix is of great importance to the analysis of dynamical systems. When analyzing the Jacobian matrix, we need to obtain the equilibrium points of the system by solving equations {$0 = f(x, y, p), 0 = g(x, y, p)$} simultaneously at first. After the equilibrium points are obtained, the Jacobian matrix of the system evaluated at the equilibrium points that are mentioned. As is well known, the stability of the equilibrium points is determined by the eigenvalues of the Jacobian matrix evaluated at the equilibrium points. The stability of the equilibrium points can be judged by observing if any eigenvalue moves from the left side to the right side of the complex plane as a parameter is varied. The system can lose its stability at different forms. Two important form of instability are saddle node bifurcation and hopf bifurcation. These types of instability are investigated for the study system under single parameter variation at next sections.

4.2. Saddle-Node Bifurcation (SNB)

At a Saddle-Node Bifurcation, two equilibrium points, one has a real positive and the other a real negative eigenvalue, coalesce and disappear both the eigenvalues becoming zero at the bifurcation. In a saddle-node bifurcation, the region of attraction of the stable equilibrium point shrinks due to an approaching the unstable equilibrium point and the stability is eventually lost when the two equilibrium coalesce and disappear [32]. This implies that an SNB has a Jacobian with a simple zero eigenvalue. The saddle-node bifurcation has been linked to voltage collapse in [24], [30], [31], [33], and [34]. An important feature of the saddle-node bifurcation is the disappearance, locally, of any stable bounded solution of the dynamic system [35]. The effect of stator resistance of SCIG on saddle-node bifurcation is investigated and primary location of eigenvalue is mentioned with star sign in Figure 17.

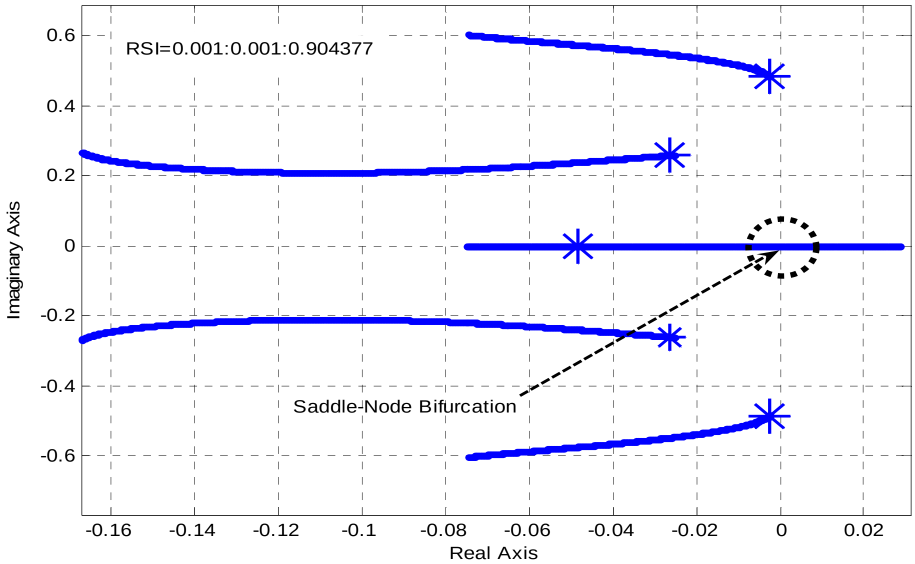

Figure 17. Eigenvalues locus with SCIG stator resistance variation

As is shown in Figure 17, stator resistance variation has a weak effect on system stability and one of the eigenvalues have moved from the left side to the right side of the complex plane. Eigenvalues varying with stator resistance variation are presented in table 1 for better observation again.

Table 1. Eigenvalues varying with stator resistance variation

R_{SI}=0.004843	**R_{SI}=0.704843**	**R_{SI}=0.724843**	**R_{SI}=0.804843**
-24.9259 + 8.4559i	-34.8192	-34.8623	-34.9892
-24.9259 - 8.4559i	-18.1585	-18.1262	-18.0306
-2.9593	-4.5977	-4.6073	-4.6368
-0.1972 + 1.6445i	-0.2644 + 1.1623i	-0.2644 + 1.1566i	-0.2644 + 1.1352i
-0.1972 - 1.6445i	-0.2644 - 1.1623i	-0.2644 - 1.1566i	-0.2644 - 1.1352i
-0.0026 + 0.4852i	-0.0622 + 0.5891i	-0.0636 + 0.5906i	-0.0686 + 0.5963i
-0.0026 - 0.4852i	-0.0622 - 0.5891i	-0.0636 - 0.5906i	-0.0686 - 0.5963i
-0.3626	-0.1577 + 0.2404i	-0.1593 + 0.2434i	-0.1640 + 0.2552i
-0.0262 + 0.2596i	-0.1577 - 0.2404i	-0.1593 - 0.2434i	-0.1640 - 0.2552i
-0.0262 - 0.2596i	-0.2161	-0.2148	-0.2113
-0.0484	**-0.0037**	**0.0000**	**0.0136**

4.3. Hopf Bifurcation (HB)

As we know, a SNB is characterized by a zero eigenvalue at the origin of the complex plane. There is another type of stable equilibrium points that can become unstable following a parameter variation that force a pair of complex eigenvalues to cross the imaginary axis in the complex plane [32]. This type of oscillatory instability is associated with nonlinear systems and it is known as Hopf Bifurcation (HB). Figure 18 shows the loci of the eigenvalues near the Hopf bifurcation point. In Figure18, the effect of rotor inductance of squirrel cage induction generator on Hopf-Bifurcation is investigated.

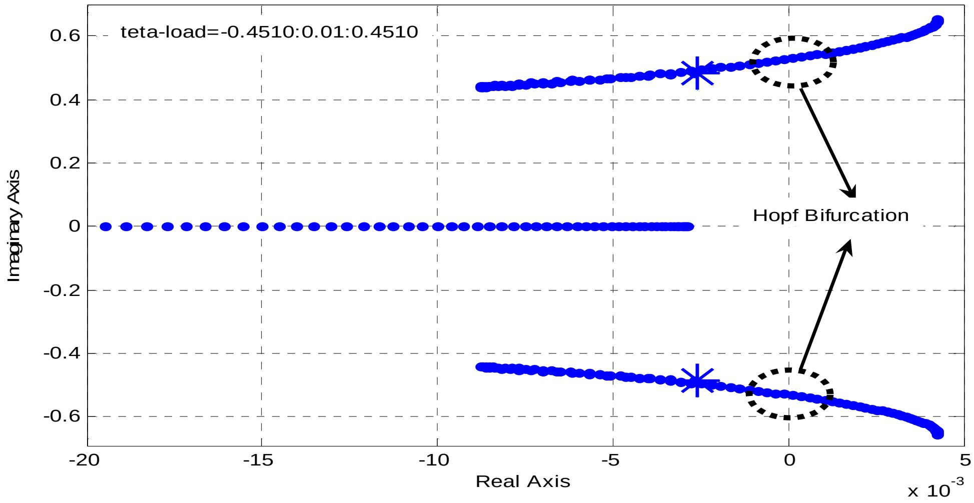

Figure 18 Eigenvalues locus with rotor inductance variation

Eigenvalues varying with rotor inductance variation are presented in table 2 for better observation again.

Table 2. Eigenvalues varying with rotor inductance variation

Teta_load=0.4510	**Teta_load=0.2510**	**Teta_load= -0.2510**	**Teta_load= -0.4510**
-24.9259 + 8.4559i	-25.0194 + 8.2401i	-24.8950 + 9.0041i	-24.6927 + 9.7788i
-24.9259 - 8.4559i	-25.0194 - 8.2401i	-24.8950 - 9.0041i	-24.6927 - 9.7788i
-2.9593	-3.0991	-3.0977	-2.9445
-0.1972 + 1.6445i	-0.1943 + 1.6199i	-0.1655 + 1.6454i	-0.1401 + 1.6916i
-0.1972 - 1.6445i	-0.1943 - 1.6199i	-0.1655 - 1.6454i	-0.1401 - 1.6916i
-0.0026 + 0.4852i	**-0.0087 + 0.4414i**	**0.0028 + 0.5850i**	**0.0043 + 0.6558i**
-0.0026 - 0.4852i	**-0.0087 - 0.4414i**	**0.0028 - 0.5850i**	**0.0043 - 0.6558i**
-0.3626	-0.3661	-0.3780	-0.3792
-0.0262 + 0.2596i	-0.0349 + 0.2585i	-0.0546 + 0.2407i	-0.0554 + 0.2395i
-0.0262 - 0.2596i	-0.0349 - 0.2585i	-0.0546 - 0.2407i	-0.0554 - 0.2395i
-0.0484	-0.0318	-0.0058	-0.0029

In addition, the effect of other system parameters on Hopf bifurcation or saddle-node bifurcation can be investigated. As an example, the effect of line length on Hopf-Bifurcation is shown at Figure 19, when the line length is varied from 10 Km to 40 Km.

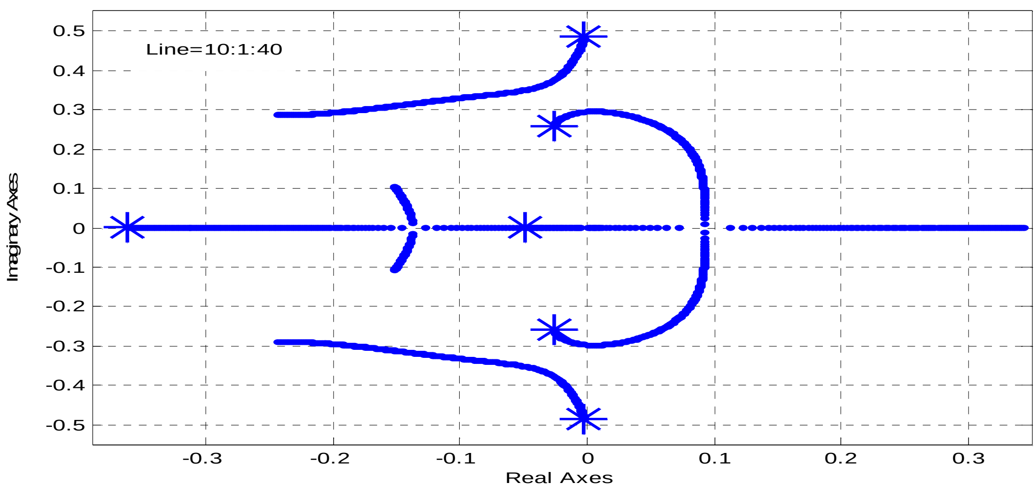

Figure 19 Eigenvalues locus with line length variation

Eigenvalues varying with line length variation are presented in table 3 for better observation again.

Table 3. Eigenvalues varying with line length variation

Line length=10 Km	Line length=15 Km	Line length=17..935Km	Line length=25 Km
-24.9259 + 8.4559i	-24.7277 + 9.2780i	-24.6119 + 9.7161i	-24.3351 +10.6635i
-24.9259 - 8.4559i	-24.7277 - 9.2780i	-24.6119 - 9.7161i	-24.3351 -10.6635i
-2.9593	-2.7764	-2.6725	-2.4321
-0.1972 + 1.6445i	-0.1967 + 1.6054i	-0.1962 + 1.5842i	-0.1943 + 1.5376i
-0.1972 - 1.6445i	-0.1967 - 1.6054i	-0.1962 - 1.5842i	-0.1943 - 1.5376i
-0.0026 + 0.4852i	-0.0154 + 0.4084i	-0.3407	-0.3171
-0.0026 - 0.4852i	-0.0154 - 0.4084i	-0.0425 + 0.3554i	-0.1194 + 0.3239i
-0.3626	-0.3492	-0.0425 - 0.3554i	-0.1194 - 0.3239i
-0.0262 + 0.2596i	**-0.0217 + 0.2765i**	**0.0000 + 0.2964i**	**0.0623 + 0.2490i**
-0.0262 - 0.2596i	**-0.0217 - 0.2765i**	**0.0000 - 0.2964i**	**0.0623 - 0.2490i**
-0.0484	-0.0413	-0.0370	-0.0261

4.4. Voltage stability

Voltage stability is defined as the ability of a power system to maintain steady voltages at all buses in the system after being subjected to a disturbance from a given initial operating condition. Voltage stability is a problem in power networks, which are heavily load, faulted, or with insufficient reactive power supply. Main reason for voltage instability is the increased of the load, for that reason, voltage stability is also called load stability problem.

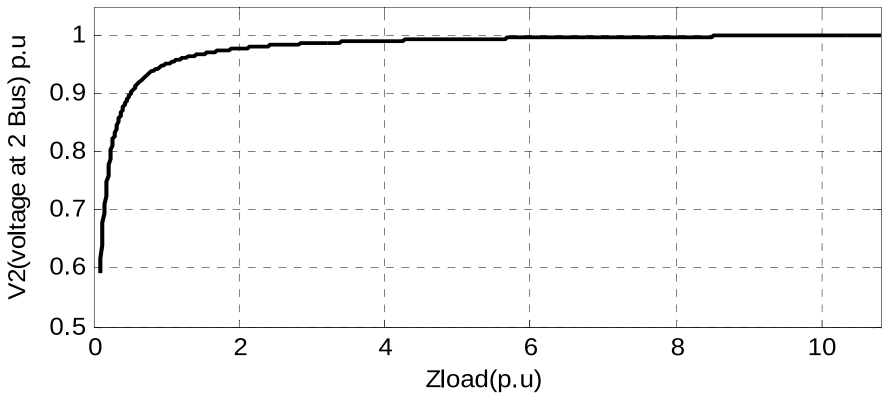

Figure 20. Voltage collapse phenomena by Z_{load}-V curve

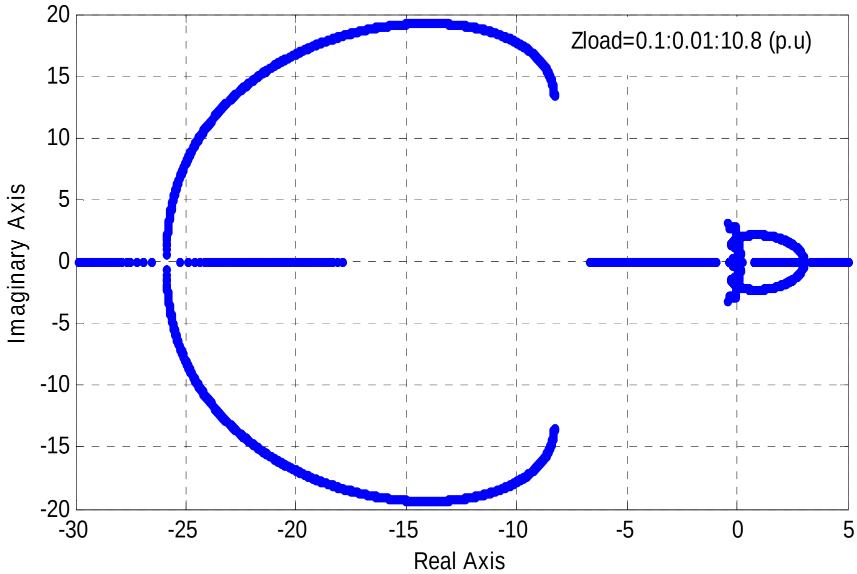

Figure 21 Eigenvalues of RJM with Z_{load} variation

Voltage Collapse is the process by which the sequence of events accompanying voltage instability leads to a blackout or abnormally low voltages in a significant part of the power system [21]. Load models are important in voltage collapse studies. The sensitivity of the loading margin with respect to parameters of a load model can be used to estimate the effect on the loading margin of using more detailed models [36]. Voltage stability is usually represented by P-V curve. In this paper, voltage collapse phenomena are shown by Z_{load}-V curve (as shown in Figure 20) that the local load is modeled by constant impedance. The nose point is called the point of voltage collapse (POVC). At this point voltage drops rapidly with an increase of the power load and Jacobian becomes singular. Power-flow solutions fail to converge beyond this limit, which indicate voltage instability and can be associated with a saddle-node bifurcation point.
In general, voltage stability can also examine by eigenvalues of RJM (see Figure 21, 22).

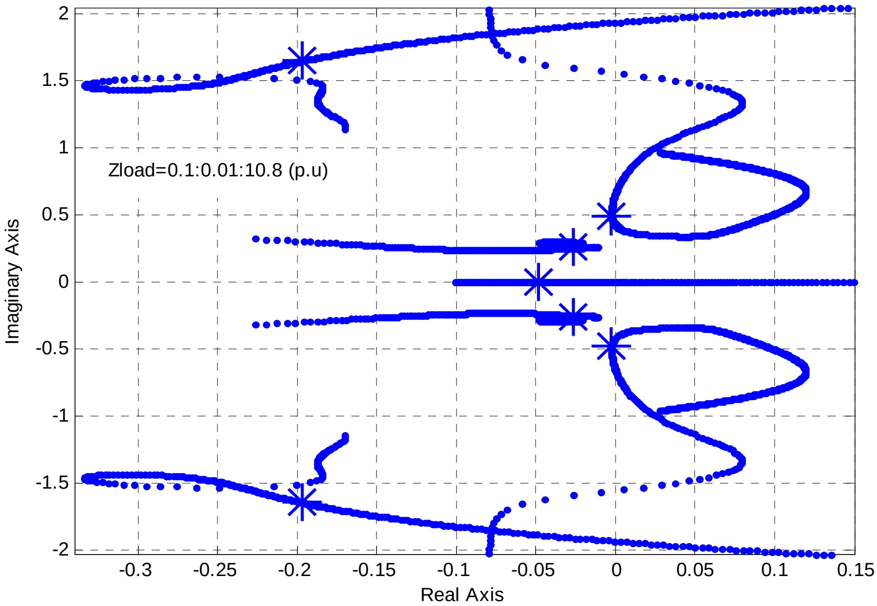

Figure 22 Eigenvalues of RJM with Z_{load} variation with zoom in eigenvalues locus near the zero

4.5. Participation Factors

The eigenvalue sensitivity with respect to a physical parameter gives an estimate of the eigenvalue shift when such parameter is changed. Thus, eigenvalue sensitivity may also be used to obtain reduced-order models of physical systems. Several methods have been proposed to analyze the connection between a system variable and its modes [37-41]. One of these methods, the participation factor approach, has been extensively used for the analysis of power systems [39, 42]. The participation factors are very much useful in small-signal stability analysis both in case of local mode and inter-area mode. The absolute value of participation factors reveals which machines are involved in a particular mode and machines could go out of step that might create problem in the power system. Participation factors are sensitivity of eigenvalues with respect to diagonal terms in RJM which are defined as:

$$p_{ki} = \frac{\partial \lambda_i}{\partial a_{kk}} \tag{53}$$

Where λ_i, a_{kk} are the ith eigenvalue and kth diagonal element in RJM. When all the eigenvalues are calculated, it is also possible to obtain the participation factors and it is evaluated in the following way. Let V and W be the right and left eigenvector matrices respectively, such that:

$$Av_i = \lambda_i v_i \tag{54}$$

$$w_i^t A = w_i^t \lambda_i \tag{55}$$

Then the participation factor P_{ij} of the kth state variable to the ith eigenvalue can be defined as:

$$p_{ki} = \frac{w_{ki}\, v_{ik}}{w_i^t\, v_i} \tag{56}$$

In case of complex eigenvalues, the amplitude of each element of eigenvectors is used [24]:

$$p_{ki} = \frac{|v_{ik}||w_{ki}|}{\sum_{k=1}^{n} |v_{ik}||w_{ki}|} \tag{57}$$

In this section participation factor for two scenarios are investigated in tables 4 and 5.

Table 4. Participation factors in Stable operation

Eigenvalue / *State Variables*	**-24.6119 + 9.7161i**	**-24.6119 - 9.7161i**	**-2.6725**	**-0.1962 + 1.5842i**	**-0.1962 - 1.5842i**	**-0.3407**	**-0.0425 + 0.3554i**	**-0.0425 - 0.3554i**	**0.0000 + 0.2964i**	**0.0000 - 0.2964i**	**-0.0370**
omega_t ($\times 10^{-4}$)	0.0000	0.0013	0.0001	0.0089	0.0002	0.0001	**0.3575**	**0.1043**	0.0027	0.0001	0.0977
S($\times 10^{-3}$)	0.0005	**0.1337**	0.0014	0.0382	0.0007	0.0000	**0.0407**	0.0119	0.0001	0.0000	**0.0545**
Teta_tg	0.0000	0.0000	0.0000	0.0001	0.0000	0.0000	0.0003	0.0000	0.0000	0.0000	**0.0012**
beta_i	0.0127	**0.1353**	0.0247	0.0287	0.0004	0.0009	0.0064	0.0006	0.0017	0.0016	**0.4390**
e_D	0.0002	**0.0024**	0.0007	0.0004	0.0000	0.0001	0.0001	0.0000	0.0000	0.0000	0.0008
e_Q ($\times 10^{-3}$)	0.0963	0.0708	**0.4156**	**0.8532**	**0.1298**	0.0003	**0.1209**	0.0189	0.0052	0.0199	0.0354
E_D	**0.5259**	**0.1489**	0.0989	0.0066	0.0001	0.0001	0.0023	0.0005	0.0005	0.0015	0.0081
E_Q	**0.1541**	0.0436	0.0105	0.0006	0.0000	0.0000	0.0005	0.0001	0.0001	0.0003	0.0014
Omega	**0.0040**	0.0004	**0.0051**	**0.0018**	0.0000	0.0000	0.0005	0.0001	0.0001	0.0002	0.0001
delta	0.0002	0.0000	**0.0023**	**0.0017**	0.0000	0.0000	**0.0015**	0.0003	0.0002	0.0007	**0.0034**
E_{fd}	**0.3028**	**0.4202**	**0.7742**	**0.9559**	0.0018	0.0001	0.0170	0.0030	0.0001	0.0070	0.0622

Table 5. Participation factors in Hopf -Bifurcation occurrence with line length variation

Eigenvalue / *State Variables*	**-24.9259 + 8.4559i**	**-24.9259 - 8.4559i**	**-2.9593**	**-0.1972 + 1.6445i**	**-0.1972 - 1.6445i**	**-0.0026 + 0.4852i**	**-0.0026 - 0.4852i**	**-0.3626**	**-0.0262 + 0.2596i**	**-0.0262 - 0.2596i**	**-0.0484**
omega_t ($\times 10^{-4}$)	0.0000	0.0014	0.0001	0.0099	0.0002	0.0001	**0.2105**	0.0929	0.0051	0.0002	**0.2002**
S($\times 10^{-3}$)	0.0008	**0.1086**	0.0012	0.0466	0.0008	0.0000	0.0599	0.0310	0.0001	0.0000	**0.0976**
Teta_tg	0.0000	0.0000	0.0000	0.0001	0.0000	0.0000	0.0003	0.0000	0.0000	0.0000	**0.0016**
beta_i	0.0131	**0.1099**	0.0206	0.0357	0.0004	0.0003	0.0023	0.0009	0.0039	0.0035	**0.4466**
e_D	0.0002	**0.0020**	0.0006	0.0004	0.0000	0.0000	0.0001	0.0001	0.0000	0.0000	0.0009
e_Q ($\times 10^{-3}$)	**0.1012**	0.0512	**0.4228**	**0.3386**	0.0159	0.0111	**0.1600**	0.0176	0.0194	0.0417	**0.2008**
E_D	**0.2873**	**0.1453**	0.0644	0.0023	0.0001	0.0002	0.0024	0.0006	0.0008	0.0017	0.0071
E_Q	**0.1273**	0.0755	0.0079	0.0009	0.0001	0.0000	0.0006	0.0001	0.0000	0.0001	0.0012
Omega	**0.0071**	0.0003	**0.0070**	0.0040	0.0000	0.0000	0.0008	0.0000	0.0000	0.0001	0.0000
delta	0.0003	0.0000	**0.0028**	**0.0037**	0.0000	0.0000	0.0018	0.0001	0.0001	0.0004	**0.0024**
E_{fd}	**0.5645**	**0.4892**	**0.7970**	**0.9482**	0.0019	0.0004	0.0146	0.0024	0.0001	0.0048	0.0463

From tables four and five can easily investigate state variables effect on eigenvalues that is bolded in each column of tables.

5. CONCLUSION

In this paper, wind-diesel system is modeled by a set of nonlinear first order differential and algebraic equations and the proposed dynamic model investigates dynamic behavior of the system. The proposed model is verified by simulation and eigenvalue analysis. In this paper, it is also shown that how eigenvalue based methods can be applied to dynamic stability analysis of a wind-diesel system. Using those eigenvalues, corresponding eigenvectors and participation factors are obtained. It is seen from eigenvalue analysis that the stability of the system can be analyzed by using eigenvalues locus. It is found from the eigenvalue analysis that which of the eigenvalues has positive real part, so the system is unstable and which state has the highest participation factor. Two important types of instability, i.e. saddle node bifurcation and Hopf bifurcation are analyzed by proposed dynamic model. System dynamic voltage stability is also investigated by using reduced Jacobian matrix (RJM).

List of Abbreviations

DAE Dynamic and Algebraic Equations
PI Proportional-Integral
SCIG Squirrel Cage Induction Generator
RJM Reduced Jacobian Matrix
UJM Unreduced Jacobian Matrix
SNB Saddle-Node Bifurcation
HB Hopf Bifurcation
POVC Point Of Voltage Collapse

APPENDIX A

Table (A.1). Drive Train System & Pitch Control System Parameters

Drive Train System & Pitch Control System Parameters			
K	0.55	H_g	4.5
D	0.01	K_p	5
$\mathbf{H_t}$	0.75	K_i	25

Table (A.2). Transmission line parameters

Transmission Line Parameters & $V_{base}=20^{kV}$		
R	0.1153 Ohm /km	(0.029 p.u)
L	1.05×10^{-3}	(0.099 p.u)
Length	$10^{\ km}$	

Table (A.3). Transformer Parameters

Transformer Parameters & S_{nom}=4 MVA			
$V_{primary}$	460/575 V	$R_{secondary}$	8.5×10^{-5}
$V_{secondary}$	20 kV	$L_{primary}$	6.25×10^{-4}
$R_{primary}$	8.5×10^{-5}	$L_{secondary}$	6.25×10^{-4}

Table (A.4). Synchronous generator parameters

$V_{base}=460^{volt}$, Frequency=60^{HZ} , $S_{base}=10^{MVA}$,$S_{nom}=2.5^{MVA}$			
R_s	0.017 (p.u)	T'_{qo}	0.213
x_d	3.23	H	0.3468
x_q	2.79	F	0.009238
x'_d	0.21	P	2 (Round Pole)
x'_q	1.03	T_{ex}	0.1
T'_{do}	1.7	K_{ex}	50

Table (A.5). Squirrel cage induction generator parameters

V_{base}=575^{volt}, Frequency=60^{HZ}, S_{base}=10^{MVA}, V_{wind}=9 $^{m/s}$, S_{nom}=3.33^{MVA}			
R_s	0.004843(p.u)	X_m(p.u)	2.77
R_r	0.004377(p.u)	X_r(p.u)	0.1791
X_s	0.1248(p.u)	P(pole pairs)	3

Table (A.6): Load parameters

Load parameters (V_{base}=20^{kV}, P=5^{MW})	
Z	1.8 (p.u)
Cos(φ)	0.4510
connection	Star(Y)

REFERENCES

[1] Greenpeace and European Wind Energy Association. Wind Force 12: a blueprint to achieve 12% of the world's electricity from wind power by 2020, 2004.
[2] Saad-Saoud Z, Jenkins N. Simple wind farm dynamic model. IEE Proc Gener Transm Distrib 1995; 142(5): 545–8.
[3] Akhmatov V, Knudsen H, Nielsen AH, Pedersen JK, Poulsen NK.Modeling and transient stability of large wind farms. Electr Power Energy Syst 2003; 25:123–44.
[4] Sorensen P, Anca H, Janosi L, Bech J, Bak-Jensen B. Simulation of interaction between wind farm and power system.: Riso National Laboratory; 2001 [Riso-R-1281].
[5] Papathanassiou SA, Papadopoulos MP.Dynamic behavior of variable speed wind turbines under stochastic wind. IEEE Trans Energy Conver 1999; 14(4):1617–23.
[6] Scott GW, Wilreker VF, Shaltens RK. Wind turbine generator interaction with diesel generators on an isolated power system. IEEE Trans Power App Sys 1984; 103(5):933–7.
[7] Papadopoulos M, Malatestas P, Hatziargyriou N. Simulation and analysis of small and medium size power systems containing wind turbines. IEEE Trans Power Sys 1991; 6(4):1453–8.
[8] Malatestas PB, Papadopoulos MP, Stavrakakis G. Modeling and identification of diesel–wind turbines systems for wind penetration assessment. In: IEEE/PES 1992 Summer Meeting, Seattle, WA, Paper 92 SM 411-9 PWRS.
[9] Papadopoulos M, Malatestas P, Papathanassiou S, Bilios N. Impact of high wind penetration on the power system of large islands. In: Proceedings of the European Community Wind Energy Conference (ECWEC) Lubeck-Travemunde, Germany, 1993:782–5.
[10] Choi SS, Larkin R. Performance of an autonomous diesel–wind turbine power system.Elec Power Sys Res 1995; 33:87–99.
[11] Kariniotakis GN, Stavrakakis GS.A general simulation algorithm for the accurate assessment of isolated diesel–wind turbine systems integration. Part I: a general multi machine power system model. IEEE Trans Energy Conver 1995; 10(3):577 83.
[12] Kariniotakis GN, Stavrakakis GS.A general simulation algorithm for the accurate assessment of isolated diesel–wind turbine systems integration. Part II: implementation of the algorithm and case studies with induction generators. IEEE Trans Energy Conver 1995; 10(3):584–90.
[13] Bhatti TS, Al-Ademi AF, Bansal KK. Load frequency control of isolated wind–diesel hybrid power systems. Energy Conver Manage 1997; 38(9):829–37.
[14] Das D, Aditya SK, Kothari MP.Dynamic of diesel and wind turbine generators on an isolated power system.Elec Power Energy Sys 1999; 21:183–9.
[15] Luis M. Fernandez, Jose Ramon Saenz, Francisco Jurado. Dynamic models of wind farms with fixed speed wind turbines. Renewable Energy 31 (2006) 1203–1230
[16] Freris LL. Wind energy conversion systems.UK: Prentice Hall; 1990.
[17] Siegfried Heier, "Grid Integration of Wind Energy Conversion Systems", John Wiley & Sons Ltd, 1998, ISBN 0-471-97143-X.
[18] Ledesma P, Usaola J, Rodriguez JL.Transient stability of a fixed speed wind farm. Renew Energy 2003; 28: 1341–55.
[19] Slootweg JG, Polinder H, Kling WL.Representing wind turbine electrical generating systems in fundamental frequency simulation. IEEE Trans Energy Convers 2003; 18(4):516–24.
[20] Holdsworth L, Wu XG, Ekanayake JB, Jenkins N. Comparison of fixed speed and doubly-fed induction wind turbines during power system disturbances. IEE Proc Gener Transm Distrib May 2003; 150(3):343–52.
[21] Kundur P. Power system stability and control. New York: McGraw-Hill; 1994.
[22] Brereton DS, Lewis DG, Young CC. Representation of induction motor loads during power system stability studies.AIEE Trans 1957; 76:451–61.
[23] M.A.Pai.Power System Stability.Elseiver North-Holland, Inc. Holland, 1981.
[24] P.W. Sauer and M.A.Pai.Power, Power System Dynamics and Stability, Prentice Hall, EE.UU, 1998
[25] P.M.Anderson and A.A. Fuad.Power System Control and Stability. John Willey and Sons, 2003
[26] C. Vournas, Voltage Stability of Electric Power Systems. Boston: Kluwer Academic Publishers, 1998.
[27] C. W.Taylor, Power System Voltage Stability. New York: McGraw-Hill, Inc. 1994.

[28] J. A. Momoh, M. E.El-Hawary, Electric Systems, Dynamics and Stability with Artificial Intelligence Applications.New York: M.Dekker, 2000.
[29] P.M.Anderson, A. A.Fouad, Power System Control and Stability. Piscataway, NJ: IEEE Press, 1993.
[30] G. M. Huang, L. Zhao, and X. Song,"A new bifurcation analysis for power system dynamic voltage stability studies," Power Engineering Society Winter Meeting, 2002. IEEE, vol. 2, pp. 882-887, Jan. 2002.
[31] G. M.Huang and K. Men, "Contribution allocation for voltage stability in deregulated power systems" Power Engineering Society Summer Meeting, 2002 IEEE, vol. 3, pp. 1290-1295, July 2002.
[32] S. Sastry, Nonlinear Systems: Analysis, Stability, and Control, New York: Springer- Verlag, Inc. 1999.
[33] V. Venkatasubramanian, H. Schaettler and J. Zaborazky.Local bifurcations feasibility regions in differential-algebraic systems.IEEE Trans. Automat.Cont.,vol. 40, pp.1992-2013, Dec. 1995.
[34] I. A. Hiskens and D. J. Hill, "Energy function, transient stability and voltage behavior in power systems with nonlinear loads," IEEE Trans. Power Syst., vol. 4, pp. 1525-1533, Oct. 1989.
[35] J. H Chow, P. V. Kokotovic, and Robert J. Thomas, System and Control Theory for Power Systems. New York: Spring-Verlag, 1995.
[36] Scott Greene Ian Dobson Fernando L. Alvarado," Sensitivity of the loading margin to voltage collapse with respect to arbitrary parameters", IEEE Transactions on Power Systems, vol. 12, no. 1, February 1997, pp. 262-272.
[37] M.A. El-Kady, A.A. Al-Ohaly, Fast eigenvalue sensitivity calculations for special structures of system matrix derivatives, J. Sound Vibr. 199 (3) (1997) 463–471.
[38] P.C. Brooks, R.S. Sharp, A computational procedure based on eigenvalue sensitivity theory applicable to linear system design, J. Sound Vibr. 114 (1987) 13–18.
[39] J.E. Van Ness, J.M. Boyle, F.P. Imad, Sensitivities of large multiple-loop control systems, IEEE Trans. Automat. Control AC-10 (7) (1965) 308–315.
[40] I. Takewaki, Efficient redesign of damped structural systems for target transfer functions, Compute. Methods Appl. Mech. Eng. 147 (1997) 275–286.
[41] I. Takewaki, An approach to stiffness-damping simultaneous optimization, Compute. Methods Appl. Mech. Eng. 189 (2000) 641–650.
[42] J.I. Perez-Arriaga, G.C. Verghese, F.C. Schweppe, Selective modal analysis with applications to electric power systems. Part I: Heuristic introduction. Part II: the dynamic stability problem, IEEE Trans. Power Apparatus Systems PAS-101 (1982) 3117–3134.

BIOGRAPHIES OF AUTHORS

Hamid Reza Najafi received the B. Eng and M. Eng degrees from University of Ferdowsi, Iran in 1981 and 1991, respectively and PhD from IUST, Iran in 2004. He has been a lecturer at Faculty of Engineering, University of Birjand since 1993, and he works currently as an assistant professor in Electric Power Department, Faculty of Electrical and Computer at University of Birjand, Iran. His special fields of interest include: Power System modeling, HVDC and FACTS, reliability of power system, Distributed Generation, application of ANN and fuzzy system in power system.

Farshad Dastyar received his Bachelors of engineering in electrical engineering from Guilan university, Rasht, Iran, in 2006 and master of engineering in electrical engineering from Birjand university,Birjand,Iran in 2009. He currently work at Monenco consulting engineers company (MAPNA Group). His areas of interest include Dynamic modelling of power system ,FACTS and distributed generation (DG).